THE JOURNAL OF PHYSICAL CHEMISTRY B

Article

pubs.acs.org/JPCB

Stimulated Emission Properties of Fluorophores by CW-STED Single Molecule Spectroscopy

Margaux Bouzin,[†] Giuseppe Chirico,[†] Laura D'Alfonso,[†] Laura Sironi,[†] Giancarlo Soavi,[‡] Giulio Cerullo,[‡] Barbara Campanini,[§] and Maddalena Collini*[,†]

[†]Physics Department, Università degli Studi di Milano-Bicocca, Piazza della Scienza 3, 20126, Milano, Italy

[‡]IFN-CNR, Physics Department, Politecnico di Milano, Piazza L. da Vinci 32, 20133, Milano, Italy

[§]Pharmacology Department, Università di Parma, Parco Area delle Scienze 27/A, 43124, Parma, Italy

Supporting Information

ABSTRACT: Fluorophores useful for STimulated Emission Depletion (STED) spectroscopy must fulfill strict requirements on depletion efficiency and photostability. These parameters determine the effective resolution of STED imaging. Resolution is typically measured on 30−80 nm spheres heavily decorated with STED bright fluorophores, limiting the possibility to estimate the true resolution achievable on a specific dye. Here we show how single molecule STED microscopy provides an estimate of the fluorophore stimulated emission cross section and of its photostability under STED irradiation. Fluorescein, a green and a yellow mutant of GFP, are tested, and the results are discussed and compared to those obtained with Chromeo488-covered 80 nm spheres on a commercial continuous-wave STED microscope.

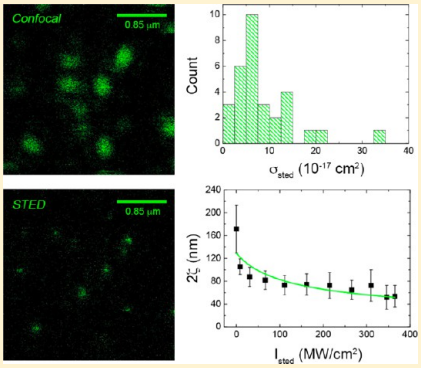

INTRODUCTION

STimulated Emission Depletion (STED) microscopy overcomes the diffraction barrier by means of light-driven depletion of the excited electronic singlet state.[1] It exploits a doughnut-shaped de-excitation beam to induce stimulated emission at the periphery of the diffraction-limited excitation spot of a scanning confocal microscope.[2,3] The superposition of the doughnut and the Gaussian beams confines the fluorescence emission to a narrow region around the central zero-intensity point of the depletion beam. Ideally, by increasing the intensity of the doughnut-shaped beam, an infinitely sharp fluorescence point-spread-function (PSF), well beyond the diffraction limit, could be obtained.[4] However, two major limitations hamper this situation: the nonperfectly zero intensity at the center of the doughnut-shaped laser beam, and the presence of processes that compete with the excited state depletion, such as reversible (blinking) and irreversible bleaching.[5]

A careful choice of the fluorescent marker is needed to exploit STED microscopy on living biological samples. First, on commercial setups, the fixed depletion wavelength (≅592 nm in this case) reduces the set of usable dyes to those with the red emission tail best superimposed with the STED line. Second, the cross section of the fluorophore for excited-state absorption either from a singlet ($S_1 \rightarrow S_{n>1}$ transition) or from a triplet state ($T_1 \rightarrow T_{n>1}$ transition) should be small.[5,6] These processes, in fact, effectively compete with spontaneous and stimulated emission, reduce the collected signal under STED imaging and may lead to bleaching.[7,8] This request is particularly demanding since STED microscopy employs high de-excitation intensity values in the red edge of the visible spectrum. In fact, Abbe's diffraction limit is reduced under depletion by a factor $\cong 1/(1 + I_{sted}/I_{sat}^{sted})^{1/2}$ where I_{sted} and I_{sat}^{sted} are the STED laser intensity and its saturation intensity, respectively.[4,9] The saturation intensity is intrinsically very high, depending on the stimulated emission cross section, $\sigma_{STED} \cong 10^{-16}-10^{-18}$ cm^2, and on the excited state lifetime $\tau_0 \cong 10^{-9}$ s, as $I_{sat}^{sted} = 1/(\sigma_{sted}\tau_0) \cong 10^{25} - 10^{27}$ events/cm^2/s.[10] This value for a 1 eV transition corresponds to about 1−100 MW/cm^2. Such high depletion intensity increases the possibility to photodamage biological samples, requires avoiding sample absorption at the STED wavelength, and may limit the optical resolution on living cells for specific dyes. Other super-resolution techniques require much lower excitation intensity,[11−13] though they are limited by a lengthy image reconstruction.

For these reasons it is extremely valuable for the application of STED microscopy to obtain a direct estimate of the resolution limit that can be reached with a specific dye. Equally relevant is the possibility of evaluating the dye robustness (inversely related to its blinking or bleaching probability at high STED intensities, I_{sted}) under repeated imaging. The setup that is commonly used to measure the stimulated emission cross sections of fluorophores is based on pump and probe spectroscopy[14] in which the gain of a probe beam is measured

Received: September 18, 2013
Revised: November 28, 2013
Published: December 3, 2013

once the molecules are primed to the excited state by a pump beam. Some studies[15,16] concerning dyes synthesized for pulsed STED laser wavelengths, dealt with the estimation of stimulated emission cross section and photostability: the derivation is, however, quite complex since the excitation and depletion beams must be synchronized, and the power of the STED pulsed beam must be varied continuously while acquiring the images.[15] More recently, STED-CW systems have been implemented[10,17] and commercialized, which require even stronger restrictions on dyes properties. We propose here a protocol to measure the effective PSF and the STED-beam profile from single-molecule fluorescence imaging with a commercial STED-CW setup and to simultaneously evaluate the photostability of the dye under the very same irradiation used for CW-STED imaging.

In this protocol, a four-state model for the dye electronic-vibrational configuration is related to the PSF in the absence and in the presence of the depletion beam, and the STED-laser doughnut profile is reconstructed thereby. We determine the STED cross section of selected fluorophores, and we also illustrate how to estimate the saturation intensity for triplet−triplet transitions that we consider as the major source for the reversible, long-lived molecular blinking observed in our STED images in CW mode.

We have tested the validity of our model on fluorescein, a widely used dye for protein labeling, and on two Green Fluorescent Protein mutants, GFP Mut2 (S65A, V68L, S72A) and its yellow analogue Mut2Y (T203Y), whose photophysical properties have already been characterized by our groups.[18,19] The protocol has been validated also on 80-nm beads stained with Chromeo 488, a specific dye for STED microscopy.[17] To further test the robustness of the results, pump and probe measurements were performed addressing the main role of stimulated emission in depleting the excited state of the tested fluorophores.

The advantages of the proposed single molecule approach are the following: it is a simple procedure to be carried out on the very same microscope to be utilized for STED measurements (no need of a devoted pump and probe setup); there is no need to label or cover with the fluorophore to be tested spheres or other structures; there are no limits to the resolution to be reached, which is limited only by the instrument; information on the STED cross section but also on the photobleaching/blinking of the dyes can be acquired, and the procedure outlined enables to reconstruct the STED PSF and the doughnut profile of the microscope.

EXPERIMENTAL AND THEORETICAL METHODS

Four-State Model. We want to describe the photodynamics of a fluorophore whose excitation is primed at λ_{exc} and whose excited state can be depleted by irradiation at λ_{sted}.The fluorophore ground state S_0 and an excited singlet state S_1 are coupled to excited vibrational states $S_{1\nu}$ and $S_{0\nu}$ (Scheme 1). Absorption, occurring at λ_{exc}, primes the transition $S_0 \rightarrow S_{1\nu}$ which vibrationally relaxes to S_1, with a typical lifetime $\tau_{vib} \sim 1-10$ ps ($k_{11} = \tau_{vib}^{-1} \sim 10^{11}-10^{12}$ s^{-1}) much faster than the typical spontaneous relaxation time from S_1 to $S_{0\nu}$, $\tau_0 = 1/\Gamma \cong 10^{-9}$ s. When the depletion beam is switched on, excited fluorophores on the state S_1 may undergo stimulated transition to $S_{0\nu}$ with emission of photons at λ_{sted}.[20] The depletion rate is typically $\sim 10^9$-10^{10} s^{-1}, much lower than the $S_{0\nu} \rightarrow S_0$ relaxation rate $k_{00} \sim 10^{11}-10^{12}$ s^{-1}. Therefore re-excitation by the STED beam to S_1 is negligible and the fast depopulation of the singlet state $S_{0\nu}$ is favored.

Scheme 1. Vibronic (Electronic Plus Vibrational) Levels Involved in the Stimulated Emission Transition[a]

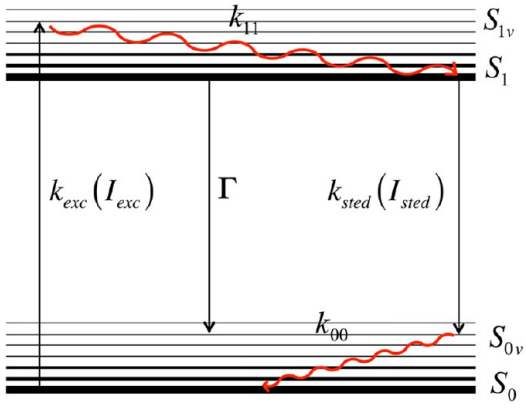

[a]The ground state vibronic level is pictured as a series of vibrational levels (S_0 is the lowest, $S_{0\nu}$ is a vibrationally excited state ν); in a similar way, the first excited vibronic singlet state is shown, where S_1 is the vibrationally relaxed and $S_{1\nu}$ a vibrationally excited level. In both cases, the wavy line depicts the transition for vibrational relaxation (rates k_{00} and k_{11}). Light excitation occurs with rate k_{exc}, dependent upon I_{exc}, from S_0 to $S_{1\nu}$. Fluorescence occurs with rate Γ from S_1 to $S_{0\nu}$ and stimulated emission occurs at rate k_{sted}, dependent upon I_{sted}, from S_1 to $S_{0\nu}$.

The rate equations for the populations of the four electronic levels in Scheme 1 can be written as

$$\begin{cases} \dfrac{dS_0}{dt} = -k_{exc}S_0 + k_{00}S_{0\nu} \\ \dfrac{dS_{0\nu}}{dt} = k_{sted}S_1 + \Gamma S_1 - k_{00}S_{0\nu} \\ \dfrac{dS_1}{dt} = k_{11}S_{1\nu} - k_{sted}S_1 - \Gamma S_1 \\ \dfrac{dS_{1\nu}}{dt} = k_{exc}S_0 - k_{11}S_{1\nu} \end{cases} \quad (1)$$

The $S_1 \rightarrow S_{0\nu}$ spontaneous relaxation rate Γ is composed of the radiative and nonradiative rates, k_R and k_{NR}: $\Gamma = 1/\tau_0 = k_R + k_{NR}$. The equilibrium solutions of eq 1 under continuous wave excitation and stimulation are:

$$\begin{cases} \bar{S}_1 = \dfrac{k_{exc}}{k_{sted} + \Gamma}\bar{S}_0 \\ \bar{S}_{1\nu} = \dfrac{k_{exc}}{k_{11}}\bar{S}_0 \\ \bar{S}_{0\nu} = \dfrac{k_{exc}}{k_{00}}\bar{S}_0 \\ 1 = \bar{S}_0 + \bar{S}_{0\nu} + \bar{S}_1 + \bar{S}_{1\nu} \end{cases} \quad (2)$$

From these equations we can write the population of the excited singlet state S_1 as

dx.doi.org/10.1021/jp409330t | J. Phys. Chem. B 2013, 117, 16405−16415

$$\overline{S_1} = \frac{k_{exc}}{k_{sted} + \Gamma}\left(\frac{1}{1 + \frac{k_{exc}}{k_{00}} + \frac{k_{exc}}{k_{sted} + \Gamma} + \frac{k_{exc}}{k_{11}}}\right) \quad (3)$$

In the following we make the assumptions that k_{00}, $k_{11} \gg \Gamma \gg k_{exc}$. In fact $k_{00} \cong k_{11} \sim 10^{11}-10^{12}$ s^{-1}, $\Gamma \cong 10^9$ s^{-1}, and $k_{exc} \cong 10^7$ s^{-1}.

Equation 3 is related to the emitted fluorescence signals in the presence, $\langle F \rangle$, and in the absence, $\langle F_{conf} \rangle$, of the depletion beam, through the radiative rate constant. We can also write the fluorescence signal as proportional to the fluorescence point-spread-function (PSF) measured in the presence and in the absence of the STED beam (PSF_{sted} and PSF_{conf}, respectively):

$$\begin{cases} \langle F \rangle = k_R \overline{S_1} = \dfrac{k_R k_{exc}}{k_{exc} + k_{sted} + \Gamma} \propto PSF_{sted} \\ \langle F_{conf} \rangle = \langle F \rangle_{k_{sted}=0} = \dfrac{k_R k_{exc}}{k_{exc} + \Gamma} \propto PSF_{conf} \end{cases} \quad (4)$$

From eq 4 we can then write k_{sted} as a combination of the PSFs. We also recall that the excitation and stimulation rates, k_{exc} and k_{sted}, are position-dependent and determined by the corresponding cross sections of the fluorophore and the intensity of the excitation and depletion beams, through

$$k_{exc}(x, y) = \sigma_{exc} I_{exc}(x, y) = \sigma_{exc} I_{0exc} f_{exc}(x, y)$$
$$k_{sted}(x, y) = \sigma_{sted} I_{sted}(x, y) = \sigma_{sted} I_{0sted} f_{sted}(x, y) \quad (5)$$

In eq 5 the functions $f_{exc}(x,y)$ and $f_{sted}(x,y)$ are the shapes of the excitation and stimulation beams, normalized to their maxima (I_{0exc} and I_{0sted}, respectively). Therefore the spatial profile of the depletion rate is finally given by

$$k_{sted}(x, y) = \sigma_{sted} I_{0sted} f_{sted}(x, y) \cong \Gamma\left(\frac{PSF_{conf}(x, y)}{PSF_{sted}(x, y)} - 1\right) \quad (6)$$

Equation 6 links the normalized shape of the STED beam $f_{sted}(x,y)$ and the stimulated emission cross section σ_{sted} of the dye to the experimental measure of the confocal and STED PSFs. Therefore, the cross section values can be inferred from images of subresolved sized fluorescent objects, acquired sequentially on the same field of view in the absence of the depletion beam (traditional confocal setup) and in the presence of both beams. According to eq 6, the procedure adopted is to measure the PSFs on subresolved objects under various level of STED-laser intensity and to compute the rate constant $k_{sted}(x,y)$ from the ratio $PSF_{conf}(x,y)/PSF_{sted}(x,y)$ and from an independent measure of the excited state lifetime of the fluorophore. The computation is generally performed along the single x-direction because the excitation and depletion rates are symmetric in the xy-plane. Finally, the determination of the stimulated emission cross section σ_{sted} can be obtained from the shape of depletion rate profile and an accurate measurement of the STED-laser intensity I_{0sted}.

STED Setup. A Leica STED-CW microscope (TCS STED CW, Leica Microsystems, Wetzlar, Germany) was employed here. This model enforces continuous-wave depletion that reduces the technical hurdles of pulsed configurations,[17] with excellent super-resolution power and limited photobleaching.

Chromophores absorption was primed by either the 488-nm or the 514-nm line of a vertically polarized Argon ion laser, and a red-shifted 592-nm circularly polarized laser induced depletion. A dedicated objective (HCX PL APO 100x/1.4 OIL STED orange, Leica Microsystems, Wetzlar, Germany) focalized the excitation (Gaussian shape) and depletion (doughnut shape) beams onto the specimen and collected the emitted signal in epi-fluorescence geometry. Confocal detection (pinhole size = 152 μm $\cong$ 1 Airy disc) was accomplished by high-sensitivity Hybrid detectors: reflected light and stimulated emission were rejected by the AOBS (Acousto-Optical Beam Splitter) coupled to a specific Notch filters set.

The excitation intensity in the focal plane was obtained as the ratio of the laser power to the beam spot area, estimated according to the explicit expression of the profile $f_{exc}(x,y)$:

$$f_{exc}(x, y) = \exp\left(-\frac{(x - x_0)^2 + (y - y_0)^2}{2\omega^2}\right) \quad (7)$$

In eq 7 we account for a slight lateral shift (x_0,$y_0 \cong 15$ nm for our setup) between the excitation peak and the zero-intensity point of the doughnut-shaped STED beam. The variance, ω, of the excitation distribution is computed from the objective numerical aperture, NA, and the excitation wavelength, λ_{exc}, as $\omega = H\lambda_{exc}/2(NA)$. The correction factor $H = 0.61$ reduces to 0.44 according to the Rayleigh's criterion for a confocal microscope.[21] The excitation intensity was then computed from the average excitation power $<P_{exc}>$ as (h = Planck's constant, c = light speed in vacuum):

$$I_{0exc} = \frac{\langle P_{exc} \rangle}{2\pi\omega^2}\frac{\lambda_{exc}}{hc}[\text{photons/cm}^2\,\text{s}] \quad (8)$$

$\langle P_{exc} \rangle$ was measured by means of a visible-wavelength power meter (PM100, Thorlabs, USA) at the objective entrance pupil plane, where the excitation beam was limited by a diaphragm the size of the entrance pupil.

The depletion intensity I_{0sted} was estimated with a similar procedure. The shape of the doughnut can be described as

$$f_{sted}(x, y) = \exp\left(-\frac{(\sqrt{x^2 + y^2} - r_0)^2}{\xi^2}\right) \quad (9)$$

Measurements of the parameters ξ and r_0 in eq 9 are typically extracted from the intensity profiles along the image of the STED-beam spot obtained by collecting the reflected light from 80-nm gold spheres. In our case, this image yields $\xi = (142 \pm 5)$ nm, $r_0 = (225 \pm 8)$ nm and a central minimum intensity corresponding to 3% of the peak value: therefore the area of the doughnut, numerically computed (eq 9, Mathematica integration routine[22]) is $(3.6 \pm 0.2) \times 10^{-9}$ cm^2. The ratio of the average laser power (effectively comprised in the range 2−293 mW) to the computed spot area leads to intensities in the range $\sim 10^{24}-10^{26}$ photons/cm^2 s ($10^6 - 10^8$ W/cm^2).

Materials. Chromeo-covered 80 nm beads mounted on a glass coverslip have been a courtesy of Leica Microsystems Italy. This sample is used to test the resolution of the Leica TCS STED CW microscope.

Fluorescein free salt was obtained from Fluka Sigma Aldrich Chemical Co. and dissolved in Milli-Q-grade bidistilled water. GFP Mut2 and Mut2Y have been purified as described elsewhere[18] and dissolved in phosphate buffer, 50 mM ionic strength (pH = 7.6), and in 1% Mowiol 8-88 (Sigma Aldrich Chemical Co.). In order to perform single molecule measure-

dx.doi.org/10.1021/jp409330t | J. Phys. Chem. B 2013, 117, 16405−16415

Table 1. Results of the Analysis of Single Molecule Images

sample	$\tau_0 = 1/\Gamma$ [ns]	$\sigma_{sted} \times 10^{17}$ [cm^2]	ζ_{max} [nm]	I_{sat}^{sted} [MW/cm^2]	P_{sat} [mW]	$\sigma^* \times 10^{17}$ [cm^2]	$I_{sat,N}$ [MW/cm^2]
fluorescein	0.26 ± 0.03	8 ± 7	53 ± 19	116 ± 65	93 ± 52	1.1−4.5	185 ± 20
Mut2	1.04 ± 0.09	5 ± 4	80 ± 30	70 ± 50	56 ± 40	0.5−1	36 ± 6
Mut2Y	2.40 ± 0.04	0.5 ± 0.3	78 ± 31	62 ± 35	50 ± 28	0.2−0.5	190 ± 31

The stimulated emission cross section σ_{sted}, obtained according to eq 17, is shown for the three fluorophores; the maximum resolution achieved, ζ_{max}, is also reported, together with the saturation power P_{sat} and the saturation intensity I_{sat}^{sted} according to eq 18. A range of values is reported for σ^*_{sted} as described in the text. The last column shows the values of the saturation intensity due to transitions to triplet states, $I_{sat,N}$, obtained by fitting the ratio $N_{spot}^{conf}/N_{spot}^{sted}$ according to eq 19.

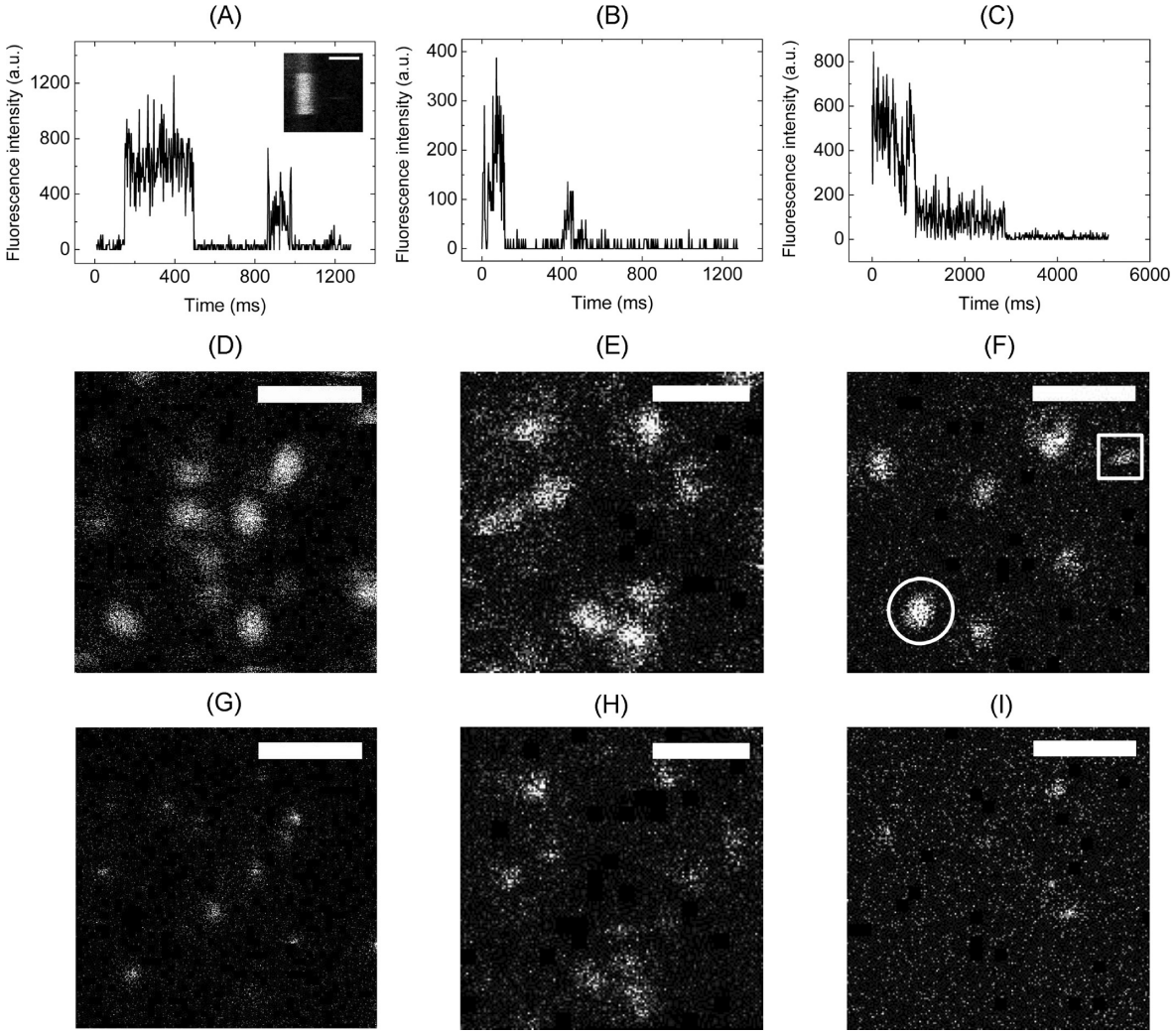

Figure 1. (A,B,C) Fluorescence intensity time traces for fluorescein, Mut2 and Mut2Y, respectively; the inset in panel A is a confocal *xt*-image obtained by repeated line scanning across a fluorescein spot (scale bar = 0.5 μm). (D,G) confocal image of single fluorescein spots and STED counterpart (P_{sted}= 54 mW, scale bar = 0.85 μm). (E,H) confocal image of single GFPMut2 spots and STED counterpart (P_{sted}= 8 mW, scale bar = 0.75 μm). (F,I) confocal image of single Mut2Y spots and STED counterpart (P_{sted}= 47 mW, scale bar = 1 μm). The square in (F) highlights a bleaching event (emission is abruptly interrupted), while the circle evidences an example of blinking (the molecule appears during the confocal scan and it disappears in the STED image, acquired sequentially as described in the text). The same scan speed (400 s^{-1}/line) has been employed for all images.

ments, the fluorophores were spin-casted at ∼100 nM concentration on a glass coverslip previously cleaned in a solution of sulphuric acid (75% v/v concentration) and oxygen peroxide (25% v/v concentration).

Fluorescence Lifetime Measurements. The fluorescence lifetimes of fluorescein, Mut2 and Mut2Y have been determined on spin coated samples on glass coverslips at μM concentration employing a frequency domain fluorometer (K2-ISS, Urbana−Champaign, IL, USA): it measures phase differences between the sample and glycogen (lifetime = 0 ns, used as reference), in the range 1−200 MHz of the modulation frequency.[23] The values obtained are reported in Table 1.

Image Acquisition in Single-Molecule Microscopy. For fluorescein and fluorescent proteins cast at nanomolar concentration on glass slides, we obtain confocal and STED images in which subresolved single spots can be discerned on a low background. These spots are ascribed to single molecules or small aggregates. This conclusion is supported by the time

fluctuations of the emitted fluorescence signal, obtained by repeated line scan across the spots. Examples of such kinetics are shown in Figure 1A–C: the fluorescence signal undergoes discrete jumps between levels that are small multiples of the intensity emitted by a single molecule.[24,25]

Each pair of confocal and STED images has been acquired sequentially on the same field of view: the STED beam is *alternatively switched on and off between lines*, so that the confocal scan of each line is immediately followed by the STED scan of the same line. This alternate sequential acquisition unravels information regarding the blinking and bleaching pathways under STED imaging. When the doughnut-shaped beam scans a spot composed of few molecules, they will either undergo stimulated emission (and therefore contribute to the reduction of the PSF) or undergo a bleaching (or long-lived blinking) event promoted by the same STED beam. In this second instance, the fluorescent spot on the STED image will either reduce its intensity (if it is an aggregate) or become completely dark (if it is a single molecule). The alternate sequential scanning allows one to discriminate between blinking and bleaching. If under this acquisition mode, in which each confocal line is acquired (sequentially) after the preceding line in the STED image, the fluorescence spot is visible in the confocal image but it is dark on the STED image, we may assume that a blinking process has taken place (Figure 1F,I). In fact the recovery time is less than the typical line acquisition time (~ms). Obviously only aggregates up to two (or three) molecules can be completely turned off by the STED beam. In fact, if N defines the aggregation order of a spot, the probability that all N molecules blink at the same time scales as $(P_{\text{blinking}})^N$, where P_{blinking} is the probability for a single molecule to undergo a blinking event.[25] This is also the reason why the effect of blinking can be neglected for Chromeo-stained 80-nm beads: the number of dye molecules on each sphere is too large to make the probability $(P_{\text{blinking}})^N$ significant. Occasionally single molecules underwent permanent bleaching (Figure 1F,I), which has a different experimental impact. In the case of blinking, the STED image loses in brightness, but the sample can be further investigated, whereas when bleaching occurs the specimen is permanently damaged.

Pump and Probe Setup. Time-resolved measurements were performed using a home-built femtosecond pump–probe spectrometer. A Ti:sapphire regenerative amplifier (Coherent Libra) was used as laser source, delivering 100 fs pulses at a central wavelength of 800 nm with 4 mJ pulse energy at a repetition rate of 1 kHz. For the excitation pulses, a single-stage optical parametric amplification (OPA), pumped at 400 nm, allows tuning the pump wavelength in the visible range, in our case λ_{exc} = 500 nm . White light generated with a 2 mm thick sapphire plate was used for probing in the visible from 450 to 780 nm. The probe transmission through the sample is measured with an optical multichannel analyzer working at the full repetition rate of the laser source.[26] The acquisition of the pump-perturbed and pump-unperturbed probe spectra allowed extraction of the differential transmission ($\Delta T/T$) of the samples. At the specific probe delay τ, it is calculated as

$$\frac{\Delta T}{T}(\lambda, \tau) = \frac{T^{\text{pump}}_{\text{on}}(\lambda, \tau) - T^{\text{pump}}_{\text{off}}(\lambda, \tau)}{T^{\text{pump}}_{\text{off}}(\lambda, \tau)} \tag{10}$$

The overall temporal resolution of the system is ≈150 fs.

RESULTS AND DISCUSSION

Validation on Chromeo488 80-nm spheres. Preliminary tests of the STED microscope resolution and of the validity of eq 6 were performed on Chromeo488-stained beads (80 nm size) excited at 488 nm. Stimulated emission depletion was obtained at increasing power, 7 < P_{sted} < 293 mW, and fluorescence was acquired through a 490–585-nm band-pass filter superimposed on a 488-nm Notch filter. Images of 19 μm × 19 μm have been acquired with a pixel size of 38 nm and with the alternate sequential acquisition mode.

A simple way to reconstruct the confocal and STED PSFs at the different STED powers is to fit the fluorescence spots corresponding to the stained beads with a Gaussian trial function $G(x,y)$ with amplitude A, variance ζ and background B:

$$G(x, y) = A \exp\left(-\frac{(x - x_0)^2 + (y - y_0)^2}{2\zeta^2}\right) + B \tag{11}$$

The PSFs for the confocal and STED acquisition mode ($\text{PSF}_{\text{conf}}(x)$ and $\text{PSF}_{\text{sted}}(x)$) given by the Gaussian fits of the spot profiles (along the x-direction and acquired on the same bead) can be employed in eq 6 to compute the radial behavior of the STED depletion rate $k_{\text{sted}}(x)$. The result of this procedure is summarized in Figure 2A. The good superposition

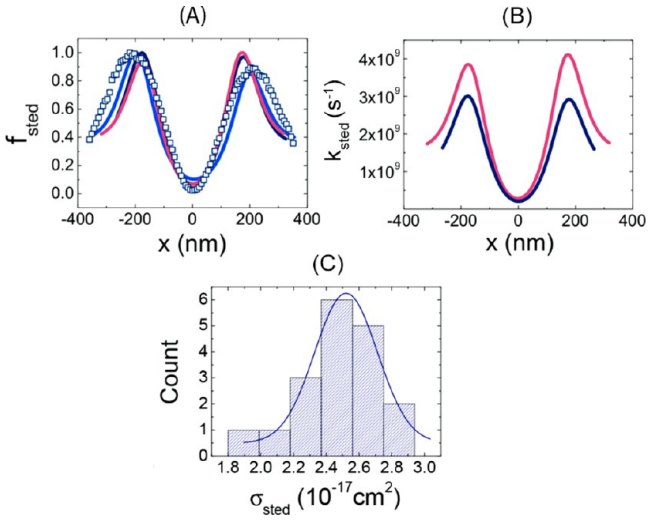

Figure 2. (A) Normalized depletion profiles (continuous lines) obtained from the PSFs of three distinct beads according to eq 6 and comparison with the profile (open squares) obtained from the reflection of the STED beam light by an 80-nm gold bead (no spatial filtering of the acquired image, pinhole size ≅ 600 μm). (B) Examples of the behavior of $k_{\text{sted}}(x)$ versus x as derived from eq 6 for two different values of the STED intensity, I_{sted} = 60 MW/cm^2 (blue, lower curve) and I_{sted} = 82 MW/cm^2 (red, upper curve). (C) Histogram of 18 values of the stimulated emission cross section obtained from Chromeo488 nanobeads: the Gaussian fit leads to $\sigma_{\text{sted}} = (2.5 \pm 0.2) \times 10^{-17}$ cm^2.

of the profiles derived from three beads, shown as examples, suggests the high level of repeatability of the reconstruction of the STED-beam shape, and the excellent agreement with the doughnut-profile obtained by collecting the reflected light of 80-nm gold beads (open squares in Figure 2A) validates the theoretical two-level model (eqs 1–6).

dx.doi.org/10.1021/jp409330t | J. Phys. Chem. B 2013, 117, 16405–16415

The profile $k_{sted}(x)$ is shown for two values of I_{0sted} in Figure 2B. By recalling eq 6, it can be related to the product of I_{0sted}, $f_{sted}(x,y)$, and σ_{sted} . Therefore, its value at the maximum, divided by I_{0sted}, gives the STED cross section σ_{sted} . The histogram shown in Figure 2C illustrates the spread of 18 recovered values of the cross section of Chromeo488.

STED Point-Spread-Functions on Single Molecules. Direct application of eq 11 to single molecules imaged through the STED microscope is limited by the number of detected photons, particularly at high STED powers. The intensity profiles derived from small aggregates or single molecule spots are often too noisy to allow a reliable reconstruction of the STED-beam shape by means of their Gaussian fit. In order to overcome this issue we have adopted an integrative evaluation of the PSF. A square Region Of Interest (ROI) is cropped around individual fluorescence spots: we denote with $G(x_k,y_j)$ the intensity of the emitted signal in the pixel of coordinates (x_k,y_j) $(j,k = 1...M$, where $M \times M$ is the number of pixels of the ROI) and we compute along the image the cumulative sum (see Scheme 2):

$$\sum_{k=(M-n+1)}^{M} \sum_{j=1}^{M} G(x_k, y_j) \equiv I(x_n) \tag{12}$$

Scheme 2. Cumulative Integration of the Signal on a Square ROI Encompassing a Single Fluorescence Spot (Dark Region)

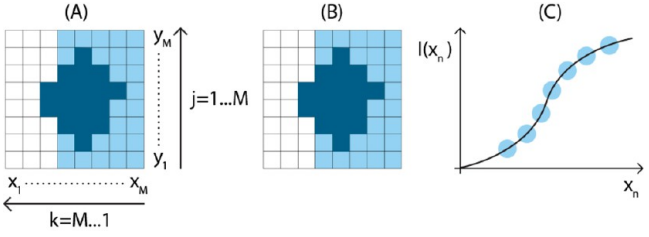

(A) Indexes k,j = 1 ... M identify each pixel (x_k,y_j), while arrows indicate the directions along which the cumulative sum is computed; the sum of the intensities of all the pixels satisfying the conditions $(M - n + 1) \le k \le M$ and $1 \le j \le M$ defines $I(x_n)$ according to eq 12; panel (B) highlights for example the pixels involved in the computation of $I(x_{n=5})$ (pixels in light blue), while panel (C) shows the trend of the cumulative sum for increasing n.

The specific integration direction does not influence the obtained result, provided that the selected spot has polar symmetry. Examples of the integrated PSFs are shown in Figure 3A, 3C, which refer to single molecules of fluorescein spin-coated on coverglass slides and imaged in both the confocal and the STED configurations. Continuous lines in the panels represent the best fit to the cumulative sum according to the trial function obtained by integrating eq 11:

$$I(x'') = A\pi\zeta^2\left[1 - \mathrm{erf}\left(\frac{x''_0 - x''}{\sqrt{2}\zeta}\right)\right] + BMx'' \tag{13}$$

A, B and ζ are the amplitude, the background, and the variance of the Gaussian function $G(x,y)$ describing explicitly the fluorescence spot (see eq 11 and Supporting Information). The intensity profiles derived along the x-direction of the single molecule spots are plotted in Figure 3B,3D and superimposed to their Gaussian fits (continuous lines). It is noteworthy that for Chromeo-labeled nanobeads, the two procedures (based on eq 11 and eq 13, respectively) provide very similar results, as shown in Figure 3E,3F, whereas for single molecules the Gaussian variance is systematically underestimated at least by a factor of 2 by the direct profile fitting method. This behavior can be ascribed to the low emission of single molecules that is digitalized by the hybrid PMT detectors in a narrow dynamic range (≈3 maximum counting on a single spot). The statistical (Poissonian) uncertainty on the data results in a systematical underestimation of the spot profile on its edge when evaluated along a single direction on the image. This problem is partly overcome by the cumulative sum performed on the ROI.

This procedure could then be applied to other relevant dyes and fluorescent proteins used in STED imaging.[27,28] In addition to fluorescein, GFPMut2 and Mut2Y embedded in Mowiol 8-88 were imaged at different STED powers. The highest resolution achieved for the three fluorophores is ζ_{max} =(54 ± 19) nm at P_{sted} = 293 mW (I_{sted} = 365 MW/cm^2) for fluorescein, ζ_{max} = (75 ± 30) nm at P_{sted} = 147 mW (I_{sted} = 183 MW/cm^2) for Mut2 and ζ_{max} = (78 ± 30) nm at P_{sted} = 147 mW (I_{sted} = 183 MW/cm^2) for Mut2Y. The different maximum powers achieved are related to the photostability of the fluorophores as discussed in the devoted section (see Figure 5).

The STED-beam profile was calculated on single molecules according to eq 6 once the confocal and STED PSF profiles were computed from the best fit of the cumulative sum. An additional issue must be considered when dealing with single-molecule spots or small aggregates. A remarkable decrease of the emitted intensity has been found in STED images even for x,y = 0, where the only expected reduction of the fluorescence signal should be attributed to the residual 3% depletion intensity at the center of the doughnut-shaped beam or to blinking. In all cases investigated here, the number of fluorescent molecules in each spot changed when going from confocal to STED imaging. If we neglect this change, the reconstructed profile $k_{sted}(x)$ would reach central values as large as 10−20% of the peak value, much higher than the value measured on Chromeo nanobeads.

Before applying eq 6 we have therefore corrected the amplitude of the profiles as follows. Let us assume that N defines the number of molecules in a given aggregate and that, due to the low excitation power used, this coincides substantially with the number of molecules contributing to the spot in the confocal image, N_{conf}. Let us also assume that N_{dark} quantifies the molecules of the aggregate that, although excited by the Gaussian-shaped beam (at the center of the doughnut), have already been pushed in a dark state by the previously scanned side of the doughnut in the scanning direction. Then, the fluorescence in the STED spot will be decreased since only $N_{sted} = (N_{conf} - N_{dark})$ molecules fluoresce.

We can then correct eq 6 for this effect by taking explicitly into account the excitation and depletion contributions at the center of the PSFs, $f_{exc}(x,y = 0)$ and $f_{sted}(x,y = 0)$:

$$\begin{cases} PSF_{conf}(0,0) \propto \dfrac{N_{conf} k_R \sigma_{exc} I_{0exc} f_{exc}(0,0)}{\Gamma} \\ PSF_{sted}(0,0) \propto \dfrac{N_{sted} k_R \sigma_{exc} I_{0exc} f_{exc}(0,0)}{\Gamma + \sigma_{sted} I_{0sted} f_{sted}(0,0)} \end{cases} \tag{14}$$

The ratio of the PSFs at (x,y) = (0,0) depends on the stimulated emission cross section and the residual STED depletion:

dx.doi.org/10.1021/jp409330t | J. Phys. Chem. B 2013, 117, 16405−16415

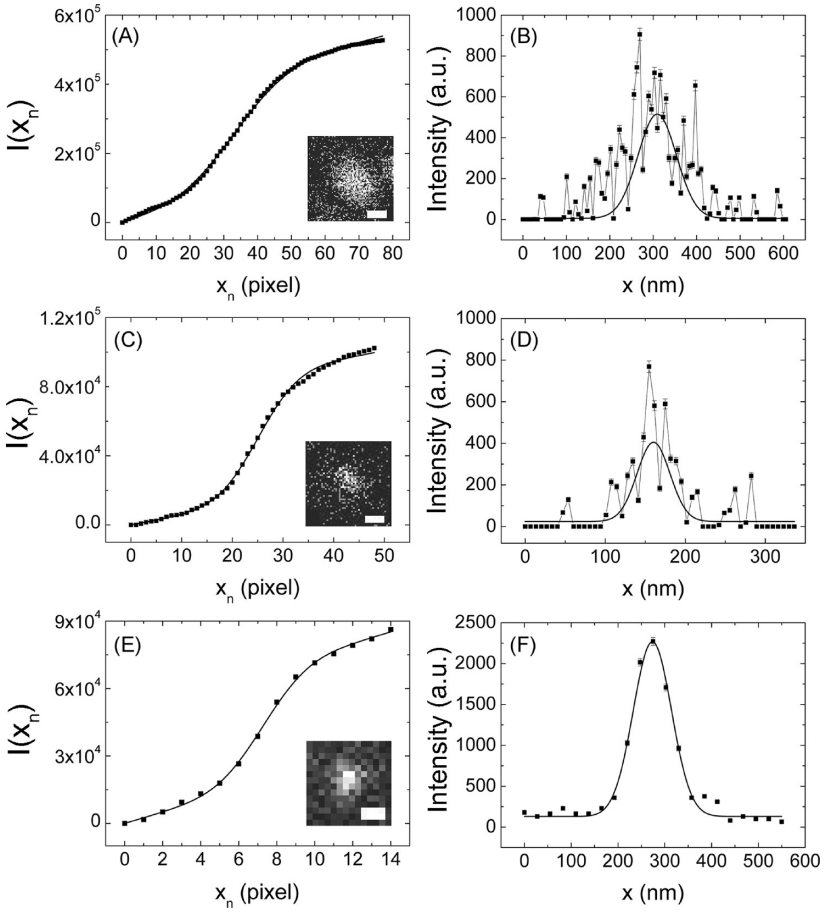

Figure 3. Comparison of the cumulative integration (eq 13, panels A,C,E) and the Gaussian fit along the central x-direction (eq 11, panels B,D,F), two methods to quantify resolution from single objects. Single fluorescein spot imaged in confocal mode (P_{sted} = 0): (A) cumulative sum fit 2ζ = (174.4 ± 0.6) nm, (B) profile fit 2ζ = (88 ± 1) nm; single fluorescein spot in STED mode (P_{sted} = 25 mW): (C) cumulative sum fit 2ζ = (83.5 ± 0.4) nm, (D) profile fit 2ζ = (41 ± 1) nm; 80-nm Chromeo bead imaged in STED configuration (P_{sted} = 293 mW): (E) cumulative sum fit 2ζ = (79 ± 1) nm, (B) profile fit 2ζ = (82 ± 1) nm. In the insets the corresponding images are also reported for reference (scale bar = 0.06 μm in A, 0.05 μm in C, and 0.11 μm in E).

$$\frac{\mathrm{PSF}_{conf}(0,0)}{\mathrm{PSF}_{sted}(0,0)} = \left(1 + \frac{\sigma_{sted} I_{0sted} f_{sted}(0,0)}{\Gamma}\right)\frac{N_{conf}}{N_{sted}} \qquad (15)$$

It can be approximated at first order to the ideal case, $f_{sted}(0,0) \cong 0$, to

$$\frac{\mathrm{PSF}_{conf}(0,0)}{\mathrm{PSF}_{sted}(0,0)} \cong \frac{N_{conf}}{N_{sted}} \qquad (16)$$

According to this approximation, eq 6, that provides us with the STED depletion profile, becomes

$$\begin{aligned} k_{sted}(x,y) &= \sigma_{sted} I_{0sted} f_{sted}(x,y) \\ &\cong \Gamma\left(\frac{N_{sted}\mathrm{PSF}_{conf}(x,y)}{N_{conf}\mathrm{PSF}_{sted}(x,y)} - 1\right) \\ &\cong \Gamma\left(\frac{\mathrm{PSF}_{sted}(0,0)\mathrm{PSF}_{conf}(x,y)}{\mathrm{PSF}_{conf}(0,0)\mathrm{PSF}_{sted}(x,y)} - 1\right) \end{aligned} \qquad (17)$$

We have applied eq 17 to the PSFs reconstructed on individual single molecules by the cumulative analysis of the intensity profiles (see eq 13). For each fluorescent spot, the STED doughnut profile has been recovered and normalized to the corresponding STED-beam intensity. The profiles measured on the three fluorophores are in very close agreement (see inset in Figure 4B). A comparison between the profiles obtained in this way and the one measured on Chromeo-covered nanospheres (Figure 2A) indicates that the latter is larger at the center, and this finding suggests that its shape is limited by the size of the nanospheres.

The values of σ_{sted} obtained on single molecules are shown through histograms in Figure 4 for the cases of fluorescein (panel A), Mut2 (panel B), and Mut2Y (panel C). The spread of the values should not be ascribed to a large uncertainty on the data (we have estimated that each individual recovered value of the STED cross section is only affected by a 2% uncertainty), but to the photoselection affecting molecules immobilized on surfaces.[29,30] In fact, the photoselection effect, which is present also with circular polarization of the STED beam, allows us to determine only the radial projection of the cross section defined as $\sigma_{rad} = \sigma_{sted} \cos^2\phi$, where ϕ is the angle formed by the molecule dipole and the focal plane.[15] Therefore the average value reported in Table 1 for each fluorophore is decreased by this effect, and the largest values found, shown in the histograms, should be closer to the true values σ_{sted}.

In the literature, comparable values of σ_{sted} as those recovered here for the investigated fluorophores have been found. In particular, for GFP mutants, values of σ_{sted} =(1.5−0.5) 10^{-16} cm^2 for EGFP in the wavelength range 550−570 nm, and σ_{sted}

dx.doi.org/10.1021/jp409330t | J. Phys. Chem. B 2013, 117, 16405−16415

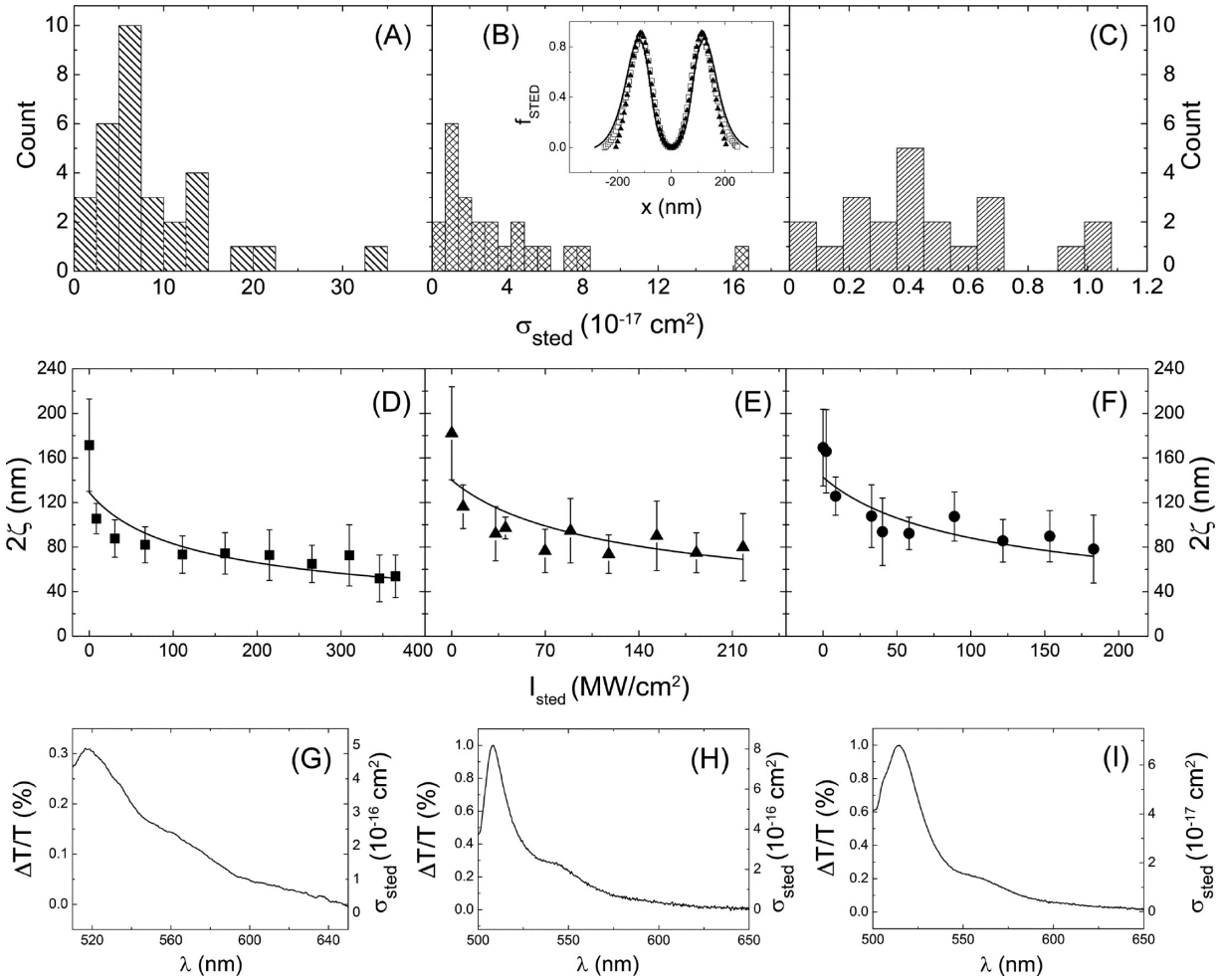

Figure 4. Fluorophores characterization: fluorescein (A, D, G), GFPMut2 (B, E, H), and Mut2Y (C, F, I). Panels A–C: Histograms of the stimulated emission cross section as derived from eq 17, whose average values are reported in Table 1. Inset in panel B: comparison among the average normalized depletion profiles obtained for fluorescein (open squares), Mut2 (continuous line) and Mut2Y (full triangles) through eq 17. Panels D–F: resolution as a function of the depletion intensity, measured according to eq 13. Solid lines are the best fits according to eq 18. Panels G–I: differential transmission spectra and STED cross section spectra obtained by pump and probe spectroscopy.

= (2–0.4) 10^{-16} cm^2 for EYFP in the wavelength range 560–600 nm are reported,[31] and values σ_{sted} =1.4 × 10^{-16} and 3.6 × 10^{-16} cm^2 for fluorescein in methanol and ethylene glycol, respectively, at 580 nm[32] have been derived. Therefore this protocol, which can be carried out on a commercial STED-CW microscope, can be extended with confidence to test dyes with unknown STED properties.

From the data presented, one can also analyze the behavior of the variance recovered through eq 13 versus increasing values of the depletion intensity (Figure 4D–F). The variance, which quantifies the radial resolution, is described by the well-known modified Abbe expression:[33,34]

$$2\zeta \cong \frac{\lambda_{exc}}{NA}\frac{1}{\sqrt{1 + I_{sted}/I_{sat}^{sted}}} \qquad (18)$$

where NA is the numerical aperture of the objective and I_{sat}^{sted} is the saturation intensity at which the probability of depletion of the excited state is equal to the probability of de-excitation via radiation. Reports in the literature[4,10,35] assume that I_{sat}^{sted} is simply related to the excited state lifetime, τ_0, and to the STED cross section, σ_{sted}, according to I_{sat}^{sted} =1/(τ_0 σ_{sted}). A low value of I_{sat}^{sted} should be advisable for efficient STED applications, but this criterion alone is not sufficient to identify efficient STED dyes, since also photostability is a crucial point that must be taken into account, as will be shown when discussing the data of Figure 5. The values of I_{sat}^{sted}, P_{sat} and ζ_{max} obtained through eq 18 for fluorescein, Mut2 and Mut2Y are shown in Table 1.

Equation 18 is approximated on several levels. It does not contain dependence on the STED wavelength and on the shape of the doughnut (in particular on the ratio of the radius to the crest width). Moreover, it depends on the correction factor for the diffraction by a circular aperture; therefore a dependence of the recovered I_{sat}^{sted} on the value of the experimental confocal resolution (I_{sted} = 0) is found. This affects the estimates of the average STED cross-section σ^*_{sted} that we can obtain from the values of I_{sat}^{sted}. A comparison of these values with those obtained through the PSF analysis (eq 6) reveals that the order of magnitude of the recovered cross section values is substantially correct. However, a large degree of uncertainty on σ^*_{sted} is given by the uncertainty in the $I_{sted} \rightarrow 0$ limits in Figure 4D–F. In fact, quite different values of I_{sat}^{sted} can be recovered if the initial (confocal) value of the resolution is fixed in the fitting procedure or not, or if the fit is performed on the data at moderate STED intensities or on the whole investigated range.

dx.doi.org/10.1021/jp409330t | J. Phys. Chem. B 2013, 117, 16405–16415

For this reason, in Table 1 we report a range of values for σ^*_{sted}, which depends upon how the fit is performed.

Nevertheless, eq 18 can be very useful for estimating and comparing the resolution that can be achieved in the case of biological samples stained with different fluorophores at high concentrations, where the signal-to-noise ratio is not affected by the limited number of photons acquired.

Pump and Probe Spectroscopy. Pump−probe spectroscopy[36] has been employed on fluorescein, GFPMut2, and Mut2Y in order to confirm the greatest role played by the stimulated emission process in depleting the excited state by measuring the $\Delta T/T$ spectrum at different pump−probe delays. The results are shown in Figure 4G−I for a pump−probe delay of 100 ps. The positive values of the $\Delta T/T$ signal suggest that stimulated emission is the dominant effect for each investigated fluorophore, since an excited state absorption to states higher than S_1 would correspond to a negative feature in the $\Delta T/T$ signal.[5] Therefore all the three fluorophores are suitable for STED application. The measurement of the $\Delta T/T$ spectrum also allows evaluating the STED cross section over the whole stimulated emission band, by normalizing the values of $\Delta T/T$ at 592 nm to unity and then multiplying them by the cross-section values derived from single molecule measurements (second column of Table 1). The results of this normalization are shown in Figure 4G−I, right scale values.

STED Induced Photobleaching on Single Molecules. Blinking or photobleaching caused by the depletion beam largely limits the applicability of CW-STED. We have performed combined studies of confocal and STED images on single molecules, acquired in alternate sequential line mode in order to estimate the resistance of selected fluorophores. We observed that some molecules lost emission under STED irradiation (Figure 1D−I) recovering the emission under pure confocal excitation, thereby undergoing blinking. Occasionally single molecules underwent permanent bleaching and could not be recovered in the confocal channel of the alternate sequential line scanning (Figure 1F). We can estimate an average of 15% bleached molecules for the three fluorophores at a STED power $P_{sted} \sim 65$ mW.

An estimate of how the blinking process is limiting the use of high intensities of the depletion beam in a CW-STED configuration can be obtained by counting the number of spots in a confocal image (N^{conf}_{spot}) and in the STED analogue (N^{sted}_{spot}), obtained by sequential line scanning, at increasing STED intensity. The ratio $N^{sted}_{spot}/N^{conf}_{spot}$ versus I_{sted}, shown in Figure 5 for fluorescein, Mut2, and Mut2Y, has a pronounced decreasing behavior.

The trend can be very well described by a simple saturation law of the type

$$\frac{N^{sted}_{spot}}{N^{conf}_{spot}} = \frac{1}{1 + \frac{I_{sted}}{I_{sat,N}}} \qquad (19)$$

on a wide range of intensity values, 10^{25} cm^{-2} s$^{-1} \leq I_{sted} \leq 10^{27}$ cm^{-2}s^{-1}. The saturation intensity indicates the 50% drop in the counted single molecules. Its value (see Table 1) is larger than I^{sted}_{sat} for fluorescein and YFP but clearly lower than I^{sted}_{sat} for GFPMut2. Therefore although GFP Mut2 has a STED cross section larger than the yellow mutant, the latter is much more resistant to photodamage at 592 nm.

It is remarkable that the simple saturation law of eq 19 fits the reduction of the number of molecules observed per image.

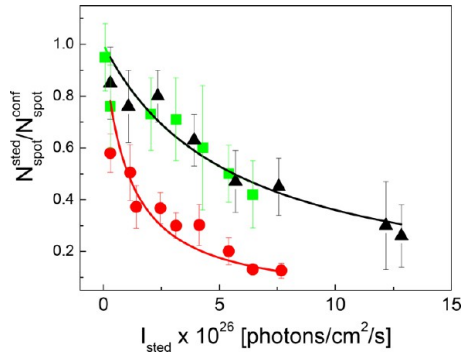

Figure 5. Relative reduction of the number of emitting objects under STED imaging with respect to pure confocal excitation ($I_{sted} = 0$), as a function of I_{sted}. Standard deviations are used as error bars. Solid lines are the best-fit curves to eq 19. Symbols refer to the case of fluorescein (triangles), Mut2 (circles), and Mut2Y (squares).

Blinking processes have been previously studied for fluorescein[37] and GFP mutants,[19,38−40] and they can occur via photoinduced transitions to long-lived high energy states.[41] Due to the lack of a clear excited state absorption band, as confirmed by the pump and probe experiments, we suggest that these transitions, primed by the STED laser, may occur from the excited triplet state ($T_1 \rightarrow T_{n>1}$).[8]

■ CONCLUSIONS

By investigating single molecules entrapped in a polymer matrix on a conventional CW-STED microscope, we are able to estimate the stimulated emission cross section and the photostability under STED illumination.

Stemming from a four-state level system, we have derived a simple relation that allows estimating the STED doughnut profile by measuring the PSFs in the presence and in the absence of the depletion beam. The STED-beam profile obtained from single molecules (or small number aggregates) in the case of widely used dyes (fluorescein) agrees well with that found for fluorescent proteins mutants (GFP Mut2 and Mut2Y). A quantitative estimate of the fluorophores cross sections is also given.

Pump and probe spectroscopy indicates that stimulated emission is the main process occurring at the excited state over the whole emission band for the fluorophores investigated here. However, the blinking on/off mechanism is found to be severe in the case of GFP Mut2 when compared to the yellow mutant or to fluorescein, suggesting that the estimate of this effect can be crucial to identify efficient dyes for STED microscopy and must be taken into account in addition to the saturation STED intensity, since it could limit the range of STED-beam intensities that can be used in order to reach the highest resolution.

■ ASSOCIATED CONTENT

Supporting Information

The details of the derivation of eq 13 can be found in the Supporting Information. This information is available free of charge via the Internet at http://pubs.acs.org.

AUTHOR INFORMATION

Corresponding Author

*Mailing address: Physics Department, Università degli Studi di Milano-Bicocca, Piazza della Scienza 3, 20126, Milano, Italy. Tel. +390264482439; E-mail: maddalena.collini@mib.infn.it.

Notes

The authors declare no competing financial interest.

ACKNOWLEDGMENTS

We acknowledge the PRIN grant 2008JZ4MLB_003 to M.C. and MAN05-ADPQ grant to G.C.

REFERENCES

(1) Klar, T. A.; Jackobs, S.; Dyba, M.; Egner, A.; Hell, S. W. Fluorescence Microscopy with Diffraction Resolution Barrier Broken by Stimulated Emission. *Proc. Natl. Acad. Sci. U. S. A.* **2000**, *97*, 8206−8210.

(2) Hell, S. W.; Wichmann, J. Breaking the Diffraction Resolution Limit by Stimulated Emission: Stimulated-emission-depletion Fluorescence Microscopy. *Opt. Lett.* **1994**, *19*, 780−782.

(3) Keller, J.; Schönle, A.; Hell, S. W. Efficient Fluorescence Inhibition Patterns for RESOLFT Microscopy. *Opt. Express* **2007**, *15*, 3361−3371.

(4) Westphal, V.; Hell, S. W. Nanoscale Resolution in the Focal Plane of an Optical Microscope. *Phys. Rev. Lett.* **2005**, *94*, 143903.

(5) Hotta, J.; Fron, E.; Dedecker, P.; Janssen, K. P. F.; Li, C.; Mullen, K.; Harke, B.; Buckers, J.; Hell, S. W.; Hofkens, J. Spectroscopic Rationale for Efficient Stimulated-emission Depletion Microscopy Fluorophores. *J. Am. Chem. Soc.* **2010**, *132*, 5021−5023.

(6) Kasper, R.; Harke, B.; Forthmann, C.; Tinnefeld, P.; Hell, S. W.; Sauer, M. Single-molecule STED Microscopy with Photostable Organic Fluorophores. *Small* **2010**, *6* (13), 1379−1384.

(7) Widengren, J.; Chmyrov, A.; Eggeling, C.; Lofdahl, P. A.; Seidel, C. A. M. Strategies to Improve Photostabilities in Ultrasensitive Fluorescence Spectroscopy. *J. Phys. Chem. A* **2007**, *111*, 429−440.

(8) Donnert, J. K.; Keller, J.; Medda, R.; Andrei, M. A.; Rizzoli, S. O.; Luhrmann, R.; Jahn, R.; Eggeling, C.; Hell, S. W. Macromolecular-scale Resolution in Biological Fluorescence Microscopy. *Proc. Natl. Acad. Sci. U. S. A.* **2006**, *103*, 11440−11445.

(9) Harke, B.; Keller, J.; Ullal, C. K.; Westphal, V.; Schonle, A.; Hell, S. W. Resolution Scaling in STED Microscopy. *Opt. Express* **2008**, *16* (6), 4154−4162.

(10) Willig, K. I.; Harke, B.; Medda, R.; Hell, S. W. STED Microscopy with Continuous Wave Beams. *Nat. Methods* **2007**, *4*, 11:915−918.

(11) Patterson, G.; Davidson, M.; Manley, S.; Lippincott-Schwartz, J. Superresolution Imaging Using Single-molecule Localization. *Annu. Rev. Phys. Chem.* **2010**, *61*, 1:345−367.

(12) Wolter, S.; Schuttpelz, M.; Tscherepanow, M. Real-time Computation of Subdiffraction-resolution Fluorescence Images. *J. Microsc.* **2010**, *237*, 1: 12−22.

(13) Van de Linde, S.; Loschberger, A.; Klein, T.; Heidbreder, M.; Wolter, S.; Heilemann, M.; Sauer, M. Direct Stochastic Optical Reconstruction Microscopy with Standard Fluorescent Probes. *Nat. Protoc.* **2011**, *6*, 7:991−1009.

(14) Grofcsik, A.; Jones, W. J. Stimulated Emission Cross-sections in Fluorescence Dye Solutions: Gain Spectra and Excited State Lifetimes of Nile Blue A and Oxazine 720. *J. Chem. Soc., Faraday Trans.* **1992**, *88*, 1101−1106.

(15) Kastrup, L.; Hell, S. W. Absolute Optical Cross Section of Individual Fluorescent Molecules. *Angew. Chem., Int. Ed.* **2004**, *43*, 6646−6649.

(16) Dyba, M.; Hell, S. W. Photostability of a Fluorescent Marker under Pulsed Excited-state Depletion through Stimulated Emission. *Appl. Opt.* **2003**, *42*, 5123−5129.

(17) Moneron, G.; Medda, R.; Hein, B.; Giske, A.; Westphal, V.; Hell, S. W. Fast STED Microscopy with Continuous Wave Fiber Lasers. *Opt. Express* **2010**, *18*, 1302−1309.

(18) Abbruzzetti, S.; Grandi, E.; Viappiani, C.; Bologna, S.; Campanini, B.; Raboni, S.; Bettati, S.; Mozzarelli, A. Kinetics of Acid-induced Spectral Changes in the GFPmut2 Chromophore. *J. Am. Chem. Soc.* **2005**, *127*, 626−635.

(19) Bosisio, C.; Quercioli, V.; Collini, M.; D'Alfonso, L.; Baldini, G.; Bettati, S.; Campanini, B.; Raboni, S.; Chirico, G. Protonation and Conformational Dynamics of GFP Mutants by Two-photon Excitation Fluorescence Correlation Spectroscopy. *J. Phys. Chem. B* **2008**, *112*, 8806−8814.

(20) Leutenegger, M.; Eggeling, C.; Hell, S. W. Analytical Description of STED Microscopy Performance. *Opt. Expr.* **2010**, *18*, 26417−26429.

(21) Webb, R. H. Confocal Optical Microscopy. *Rep. Prog. Phys.* **1996**, *59*, 427−471.

(22) *Mathematica*, version 8.0; Wolfram Research, Inc.: Champaign, IL, 2010.

(23) Lakowicz, J. R. *Principles of Fluorescence Spectroscopy*, 2nd ed.; Kluwer Academic/Plenum Publishers: New York, 2009.

(24) Hernando, J.; Hoogenboom, J. P.; van Dijk, E. M. H. P.; Garcia-Lopez, J. J.; Crego-Calama, M.; Reinhoudt, D. N.; van Hulst, N. F.; Garcia-Parajo, M. F. Single Molecule Photobleaching Probes the Exciton Wave Function in a Multichromophoric System. *Phys. Rev. Lett.* **2004**, *93*, 236404.

(25) Wai-Tak, Y.; Hu, D.; Vanden Bout, D. A.; Barbara, P. F. Classifying the Photophysical Dynamics of Single- and Multiple-chromophoric Molecules by Single Molecule Spectroscopy. *J. Phys. Chem. A* **1998**, *102*, 7564−7575.

(26) Polli, D.; Luer, L.; Cerullo, G. High-time-resolution Pump-probe System with Broadband Detection for the Study of Time-domain Vibrational Dynamics. *Rev. Sci. Instrum.* **2007**, *78*, 103108.

(27) Willig, K. I.; Kellner, R. R.; Medda, R.; Hein, B.; Jakobs, S.; Hell, S. W. Nanoscale Resolution in GFP-based Microscopy. *Nat. Methods* **2006**, *3*, 721−723.

(28) Hein, B.; Willig, K. I.; Hell, S. W. Stimulated Emission Depletion (STED) Nanoscopy of a Fluorescent Protein-labeled Organelle inside a Living Cell. *Proc. Natl. Acad. Sci. U. S. A.* **2008**, *105*, 14271−14276.

(29) Dedecker, P.; Muls, B.; Hofkens, J.; Enderlein, J.; Hotta, J. Orientational Effects in the Excitation and De-excitation of Single Molecules Interacting with Donut-mode Laser Beams. *Opt. Express* **2007**, *15*, 3372−3383.

(30) Galiani, S.; Harke, B.; Vicidomini, G.; Lignani, G.; Benfenati, F.; Diaspro, A.; Bianchini, P. Strategies to Maximize the Performance of a STED Microscope. *Opt. Express* **2012**, *20*, 7362−7374.

(31) Rittweger, E.; Rankin, B. R.; Westphal, V.; Hell, S. W. Fluorescence Depletion Mechanisms in Super-resolving STED Microscopy. *Chem. Phys. Lett.* **2007**, *442*, 483−487.

(32) Marsh, R. J.; Armoogum, D. A.; Bain, A. J. Stimulated Emission Depletion of Two-photon Excited States. *Chem. Phys. Lett.* **2002**, *366*, 398−405.

(33) Hell, S. W. Far-field Optical Nanoscopy. *Science* **2007**, *316*, 1153−1158.

(34) Hell, S. W.; Willig, K. I.; Dyba, M.; Jakobs, S.; Kastrup, L.; Westphal, V. Nanoscale Resolution with Focused Light: STED and other RESOLFT Microscopy Concepts. *Handbook of Biological Confocal Microscopy*; Springer: New York, 2006; pp 571−579.

(35) Hell, S. W. Toward Fluorescence Nanoscopy. *Nat. Biotechnol.* **2003**, *21*, 1347−1355.

(36) Cerullo, G.; Manzoni, C.; Luer, L. Time-resolved Methods in Biophysics, 4, Broadband Pump−probe Spectroscopy System with Sub-20 fs Temporal Resolution for the Study of Energy Transfer Processes in Photosynthesis. *Photochem. Photobiol. Sci.* **2007**, *6*, 135−144.

(37) Song, L.; Hennink, E. J.; Young, T.; Tanke, H. J. Photobleaching Kinetics of Fluorescein in Quantitative Fluorescence Microscopy. *Biophys. J.* **1995**, *68*, 2588−2600.

(38) Peterman, E. J. G.; Brasselet, S.; Moerner, W. E. The Fluorescence Dynamics of Single Molecules of Green Fluorescent Protein. *J. Phys. Chem. A* **1999**, *103*, 10553−10560.
(39) Garcia-Parajo, M. F.; Segers-Nolten, G. M. J.; Veerman, J. A.; Greve, J.; van Hulst, N. F. Real-time Light-driven Dynamics of the Fluorescence Emission in Single Green Fluorescent Protein Molecules. *Proc. Natl. Acad. Sci. U. S. A.* **2000**, *97*, 7237−7242.
(40) Donnert, G.; Eggeling, C.; Hell, S. W. Major Signal Increase in Fluorescence Microscopy Through Dark-state Relaxation. *Nat. Methods* **2007**, *4*, 81−86.
(41) Eggeling, C.; Widengren, J.; Rigler, R.; Seidel, C. A. M. Photobleaching of Fluorescent Dyes under Conditions Used for Single-molecule Detection: Evidence of Two-step Photolysis. *Anal. Chem.* **1998**, *70*, 2651−2659.